Chemical and Process Engineering: New Frontiers, 2026, 47(3), e140
DOI: 10.24425/cpe.2026.928

PERSPECTIVE ARTICLE

Influence of the airfoil of a PBT impeller blade on hydrodynamics

Jacek Stelmach*[1], Andrzej Obraniak[1], Andrzej Baryga[2], Stanisław Brzeziński[2]

[1] Lodz University of Technology, Faculty of Process and Environmental Engineering, Wolczanska 213, 93-005 Lodz, Poland
[2] Lodz University of Technology, Faculty of Biotechnology and Food Sciences, Wolczanska 171/173, 93-530 Lodz, Poland

*** Corresponding author, e-mail:** jacek.stelmach@p.lodz.pl

Article info:
Received: 14 May 2026
Revised: 01 July 2026
Accepted: 07 July 2026

Abstract
The velocity distributions near pitched blade turbine impellers with blades inclined at an angle of 45° and with different blade cross-sections were determined. Then, the pumping efficiency and effectiveness of the tested impellers were calculated. The impeller with the NACA4424 profile placed with the less convex side in the direction of movement turned out to be the best. The turbulent stresses generated in the mixed liquid were too small to disintegrate microbial cells.

Keywords
airfoil; efficiency; PBT impeller; velocity profile

1. INTRODUCTION

Suspension production is a process used in industrial practice (Paul et al., 2003; Stręk, 1981; Zlokarnik, 2001) and for small concentrations of suspension (Gzowska, 2019) the mixing power is equal to the mixing power for a pure liquid. Due to rising energy prices, solutions are being sought to reduce energy consumption. In the mixing process, this can be achieved by using impeller blades, the cross-section of which is shaped like an airfoil. In this way, the mixing power P can be reduced by several percent (Stelmach and Kuncewicz, 2017; Stelmach, 2022). However, it is important that the use of the profile does not reduce the pumping capacity $\dot{V}_p$ of the impeller. Then, despite the reduction of power consumption, the efficiency of the impellers may not change, which with higher construction costs will make the use of modified impellers economically unprofitable. In terms of hydraulics, impellers with a low value of the Eu/Fl_p ratio show the highest efficiency (Stręk, 1982). On the basis of the known pumping capacity $\dot{V}_p$ and mixing power P, it is possible to determine the efficiency of the impeller (Nienow, 1997), which takes into account the ratio of the obtained effects $\dot{V}_p$ to the energy expenditure P

$$E_p = \frac{\dot{V}_p \cdot \rho}{P \cdot T^4} = \frac{Fl_p^3}{Eu} \cdot \left(\frac{D}{T}\right)^4 \tag{1}$$

where: D – impeller diameter, m, T – tank diameter, m, ρ – density of the liquid, kg/m^3, $Fl_p = \dot{V}_p/(N \cdot D^3)$ – pumping (flow) number, $Eu = P/(N^3 \cdot D^5 \cdot \rho)$ – power number.

According to Equation (1), higher efficiency means that a larger liquid stream is forced through the impeller area with the same energy expenditure (or that less energy is required to convey a given liquid stream). To determine the pumping capacity $\dot{V}_p$ of axial flow impellers, it is necessary to know the axial velocity profile $U_z(r)$ under the impeller

$$\dot{V}_p = 2 \cdot \pi \cdot \int_0^{D/2} U_z(r) \cdot r \cdot dr \tag{2}$$

where: r – radius, m, $U_z(r)$ – axial velocity profile. Most often, the analytical form of the function $U_z(r)$ is not known, and then the liquid flux can be calculated on the basis of discontinuous experimental data

$$\dot{V}_p = \sum_{i=1}^{n-1} \pi \cdot U_{z_i}(r) \cdot \left(r_{i+1}^2 - r_i^2\right) \tag{3}$$

For impellers generating axial flow, the axial velocity is proposed to be described by the relations (Uhl and Gray, 1986)

$$U_z(r) = 2 \cdot \pi \cdot k \cdot N \cdot r \quad \text{dla} \quad r < r_c \tag{4}$$

$$U_z(r) = \frac{2 \cdot \pi \cdot c \cdot N}{r} \quad \text{dla} \quad r > r_c \tag{5}$$

where r_c is the radius for which the axial velocity reaches its maximum value. On the other hand, the mean square pulsations of the axial velocity $u_z'(r)$ are given by the following two equations

$$\frac{u_z'(r)}{U_z(r)} = \frac{C}{r} \quad \text{dla} \quad r < r_c \tag{6}$$

$$\frac{u_z'(r)}{U_z(r)} = K \cdot r \quad \text{dla} \quad r > r_c \tag{7}$$

The c, C, and K coefficients depend on the type and size of the impeller, while the coefficient k depends only on the type of impeller. The values of these coefficients are determined experimentally.

© 2026. The Author(s). This is an open-access article distributed under the terms of the Creative Commons Attribution (CC-BY 4.0, https://creativecommons.org/licenses/by/4.0/), which permits unrestricted use, distribution, and reproduction in any medium, provided the original author and source are credited.

The liquid pumped downwards by the impeller acts on the bottom of the tank with an axial force F_a. A relationship between the thrust force and pumping capacity has been found, which in its dimensionless form is found to be (Fořt et al., 2013; Machado et al., 2012; Story et al., 2021)

$$Th = C_1 \cdot Fl_p^a \tag{8}$$

where: a – power exponent, C_1 – coefficient, $Th = F_a/(N^2 \cdot D^4 \cdot \rho)$ – thrust number.

According to literature data (Machado et al., 2012), the value of the power exponent is $a \approx 2$, and the coefficient $C_1 \approx 1.43$. In the own research of propeller impellers (Stelmach, 2026), the given value of the power exponent was obtained, while the C_1 coefficient had a lower value $C_1 \approx 0.80$.

When mixing biosuspensions, it becomes important to be able to prevent cell disintegration during the flow of microorganisms through the impeller area. It can be caused by the mechanical action of the impeller blades and deformations resulting from the stress generated in the liquid. Calculated on the basis of literature information (Mashmoushy et al., 1998; Shiu et al., 1999; Smith et al., 2000), the breaking stresses are $\tau = 5$ MPa for yeast and $\tau = 17.8$ MPa for bacteria. Literature information (Galletti et al., 2004) shows that the stresses generated in the liquid are too small to destroy cells, but they slow down the growth of the microbial population. A decrease in methane production was also observed with an increase in the intensity of mixing (Lebranchu et al., 2017).

The stresses associated with the velocity pulsations of the liquid in the stirred tank are referred to as Reynolds stress (Uhl and Gray, 1966). The use of the PIV method allows the determination of Reynolds stress (Stelmach and Kuncewicz, 2018), which is a function of turbulent flow fluctuations and does not depend on the viscosity of the fluid

$$\tau_{ij} = -\rho \cdot \overline{u_i' \cdot u_j'} = \begin{bmatrix} \tau_{xx} & \tau_{yx} & \tau_{zx} \\ \tau_{xy} & \tau_{yy} & \tau_{zy} \\ \tau_{xz} & \tau_{yz} & \tau_{zz} \end{bmatrix} = -\rho \cdot \begin{bmatrix} \overline{u_x'^2} & \overline{u_x' \cdot u_y'} & \overline{u_x' \cdot u_z'} \\ \overline{u_x' \cdot u_y'} & \overline{u_y'^2} & \overline{u_y' \cdot u_z'} \\ \overline{u_x' \cdot u_z'} & \overline{u_y' \cdot u_z'} & \overline{u_z'^2} \end{bmatrix} \tag{9}$$

The first character in the index indicates the direction of the axis to which the surface for which the stress is calculated perpendicular while the second character of the index indicates the direction of the force. In the case of a two-dimensional measurement, it is possible to determine only three of the six stresses defined by Equation (9).

An important parameter in the mixing process is the energy dissipation rate ε. Generally, the local turbulent energy dissipation rate may be calculated from the definition formula (Baldi et al., 2002; Delafosse et al., 2011; Tanaka and Eaton, 2007)

$$\varepsilon = \nu \cdot \overline{\frac{\partial u_j'}{\partial x_i} \cdot \left(\frac{\partial u_i'}{\partial x_j} + \frac{\partial u_j'}{\partial x_i} \right)} = \frac{1}{2} \cdot \nu \cdot \overline{\left(\frac{\partial u_i'}{\partial x_j} + \frac{\partial u_j'}{\partial x_i} \right)^2} \tag{10}$$

However, direct measurements of energy dissipation rate are difficult (Paul et al., 2003; Stelmach et al., 2005). Therefore, a simple equation is often used for isotropic velocity pulsations

$$\varepsilon = C_2 \cdot \frac{\overline{u'}^3}{D} \tag{11}$$

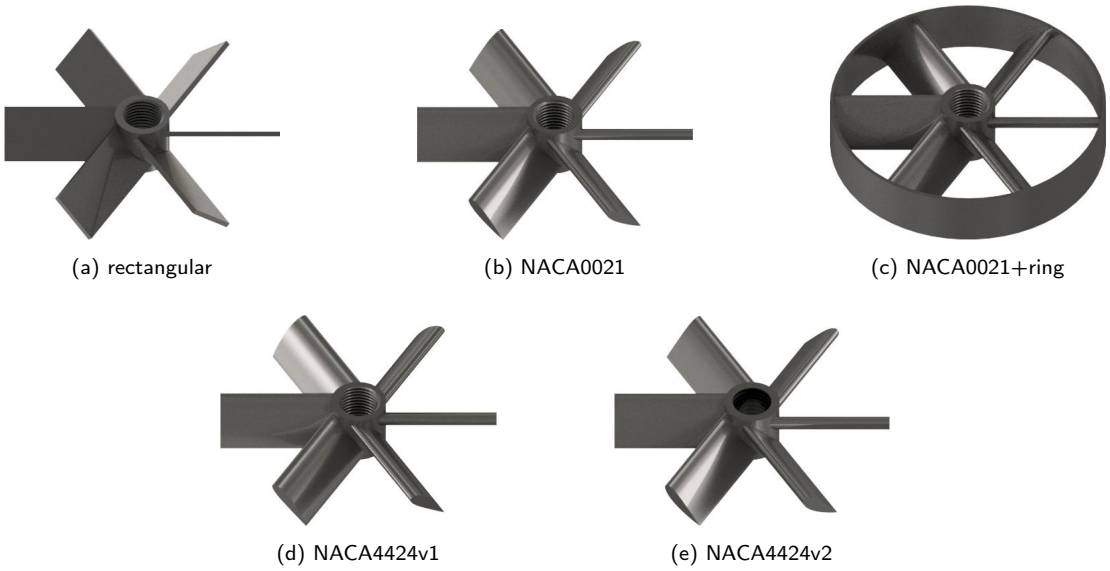
Studies show that only in a small area near the impeller we are dealing with non-isotropic turbulence (Stelmach and Musoski, 2017). The energy dissipation rate affects the size and energy of the eddies. Near the impeller, it is sufficient to break up gas bubbles (Stelmach et al., 2019). The energy dissipation rate also affects the rate of mass transfer (Linek et al., 2004).

The aim of the study was to determine the velocity fields near pitched blade turbine impellers with an airfoil cross-section of blade. On this basis, the profiles of the axial velocity under the impeller, pumping capacity and Reynolds stress would be determined. The obtained results will be the basis for determining the efficiency of the tested impellers and the impact of turbulent stresses on microorganisms.

2. MEASURING EQUIPMENT AND EXPERIMENTS

The experiment was carried out in a flat-bottomed glass tank with a diameter of $T = 292$ mm. The tank was equipped with four standard baffles ($B = 0.1 \cdot T$). The height of the liquid in the tank was $H_L = 300$ mm ($H_L \approx T$). The impeller was located at a distance of $H_m = 100$ mm ($H_m = H_L/3$) above the bottom of the tank. The impellers had a diameter of $D = 100$ mm and a attack angle of $\alpha = 45°$. Rectangular, NACA0021 and NACA4424 airfoils were used. For the last variant, two settings were used: the more convex side in the direction of movement (v2) and vice versa (v1). A impeller with a NACA0021 profile with a ring was also used. The ring should reduce radial vibrations of the shaft-impeller system (Stręk, 1981). The second goal is to test whether the ring will act as a diffuser used in screw impellers (Głogowski et al., 2024; Stręk, 1981), i.e., make the flow more axial and possibly increase the axial flow of liquid through the impeller. The tested impellers are shown in Fig. 1.

The velocity measurements were made using the LaVision PIV system (Raffel et al., 2007; Stelmach, 2014). The tests used water at a temperature of $t = 20°C$ with the addition of hollow glass spheres with an average diameter of 10 μm acting as a tracer. In PIV measurements, the liquid must be transparent, which makes it unsuitable for real suspensions. However, at low concentrations (up to 10% by mass), the influence of suspended particles on hydrodynamics is small (Gzowska, 2019). This also applies to biosuspensions, which may exhibit non-Newtonian fluid characteristics (Stelmach, 2000).



(a) rectangular (b) NACA0021 (c) NACA0021+ring

(d) NACA4424v1 (e) NACA4424v2

Figure 1. Tested impellers.

The measurement field was 75 mm × 75 mm with a camera resolution of 2048 px × 2048 px. For each impeller type, a series of 200 images were taken at rotational frequencies $N = 2, 3, 4, 6$ s^{-1}. Two-pass data processing was used to determine the velocity fields. As a result of the calculations, the values of average velocities, velocity pulsations (in RMS sense) and Reynolds stress in the horizontal and vertical directions were obtained in fields with a size of 32 px × 32 px (Raffel et al., 2007).

The tests of the pressure applied to the bottom of the stirred tank by the stream of liquid were carried out on a RADWAG WLC/30F1/R balance with a load capacity of 30 kg and an accuracy of 0.5 g. The scale was connected to the computer via an RS232 serial connector. The rotational frequency of the impellers in the range from $N = 100$ min^{-1} (1.667 s^{-1}) to $N = 600$ min^{-1} (10 s^{-1}) was changed by 50 min^{-1} (0.833 s^{-1}). After the flow had stabilized for about 30 seconds, weight readings were recorded to average the result.

3. RESULTS AND DISCUSSION

The obtained data allowed to map the average dimensionless velocities (i.e. divided by the velocity of the blade tip $U_{tip} = \pi \cdot D \cdot N$) shown as example in Fig. 2.

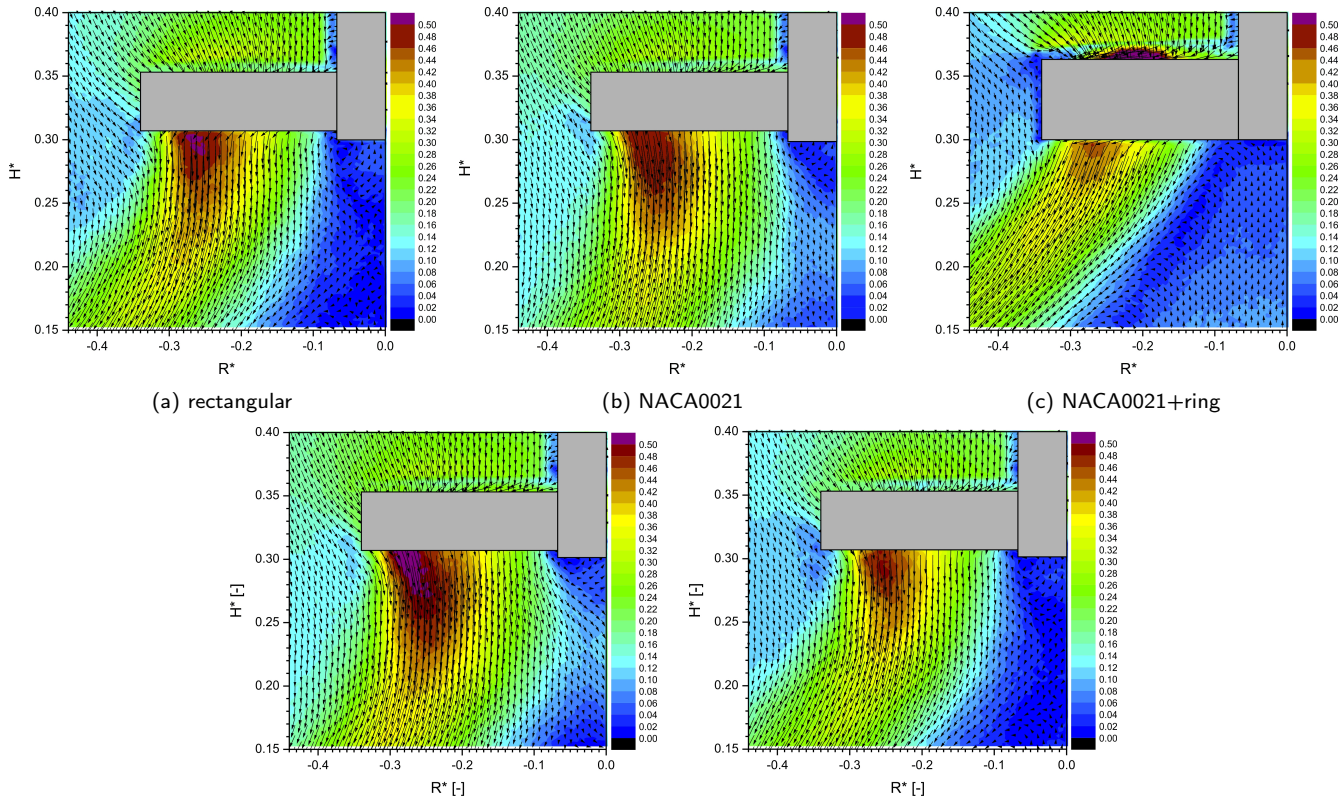
Based on the flow pattern analysis (Fig. 2), it can be concluded that all tested impellers generate axial flow. However, the ring around the impeller blocks the radial flow of liquid into the impeller. The lack of flow from the wall to the axis causes the liquid to flow radially under the influence of centrifugal force even at a short distance below the impeller. This increases the low-velocity zone under the impeller compared to impellers without a ring. When mixing suspensions, solid particles can accumulate in this zone (Mak, 1992). The maximum liquid outflow velocity from the impeller with a ring is also lower. Therefore, the ring did not meet the expectations of increasing axial flow although system vibrations were reduced. In all cases, the maximum fluid velocity occurred for approximately 2/3 of the blade length.

The distributions of dimensionless mean square velocity pulsations u' are shown in Fig. 3. In the liquid stream ejected by the impeller blades, the velocity pulsations are greater than in the stream flowing from above into the impeller. The largest pulsations occur at the lower end of the blade. The use of a ring reduced pulsations at the end of the blade.

More detailed information about the velocity distributions and velocity pulsations is provided by the component profiles at certain heights above the tank bottom. Fig. 4 shows the profiles of dimensionless velocity components and velocity pulsations. The use of dimensionless profiles made it possible to average the values for all tested rotational frequencies of the impeller.

The velocity profiles for the rectangular blade cross-section are similar to those obtained by other researchers using the LDA (Laser Doppler Anemometry) method (Kresta and Wood, 1993).

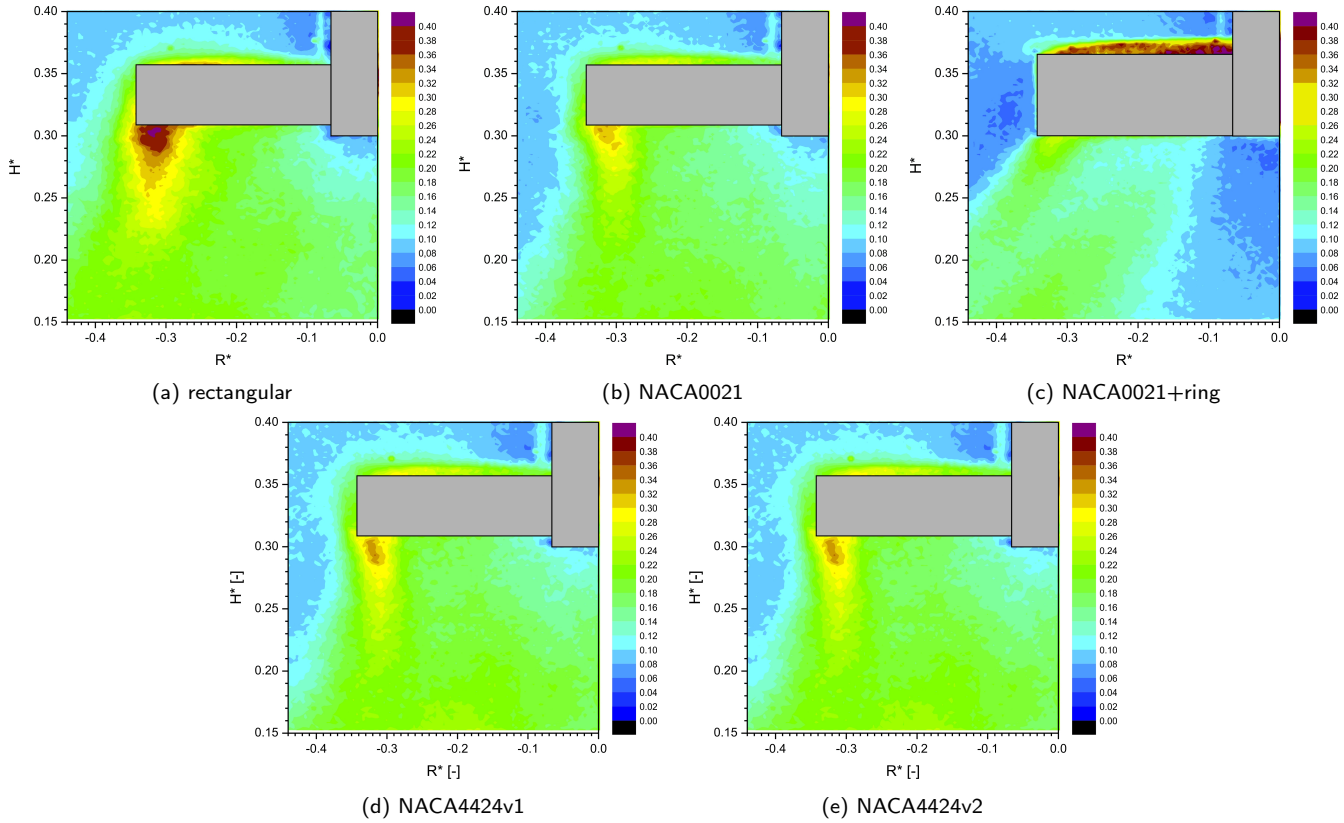
Over the impeller ($H^* = 0.380$), the axial velocity profiles are the same except for the impeller with a ring. From the course of the profiles, it can be concluded that the liquid flows relatively evenly into the impeller. The highest velocities of liquid entry into the rotor, close to $0.3 \cdot U_{tip}$, occurred in the range of $0.1 < R^* < 0.3$. Starting from $R^* \approx 0.3$ up to the tip of the blade ($R^* = 0.342$), the velocities decreased to about $0.15 \cdot U_{tip}$. For an impeller with a ring, the velocity gradient in this range R^* was higher and the velocity of entry to the rotor was smaller, as it was $0.10 \cdot U_{tip}$. In the case of the radial component above the impeller, the liquid flows in the direction of the impeller axis. The maximum value was reached for $R^* \approx 0.30$, while for the impeller with ring it was significantly higher.



(a) rectangular (b) NACA0021 (c) NACA0021+ring

(d) NACA4424v1 (e) NACA4424v2

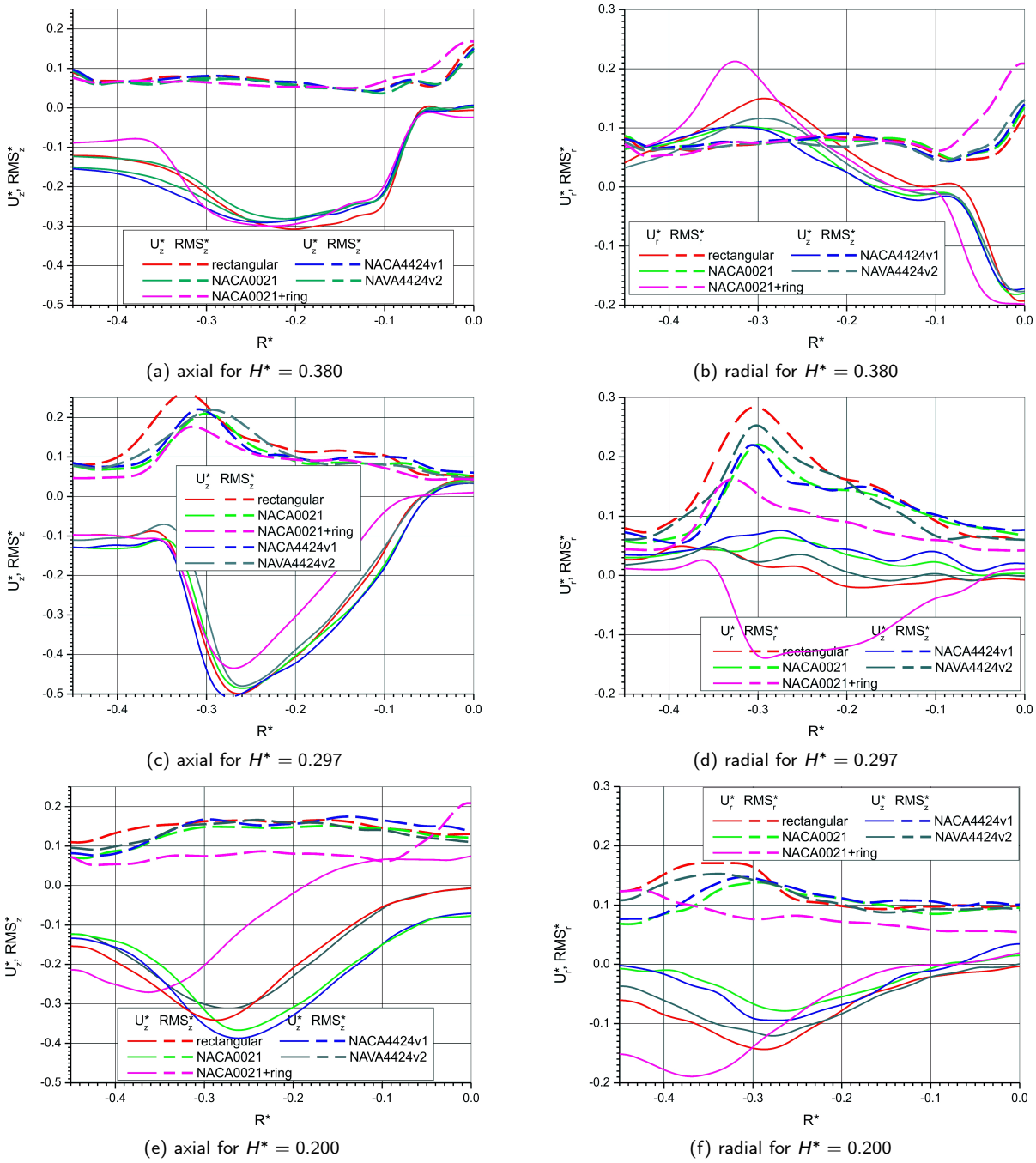
Figure 2. Dimensionless liquid velocities near the impeller, $N = 6\ s^{-1}$.



(a) rectangular (b) NACA0021 (c) NACA0021+ring

(d) NACA4424v1 (e) NACA4424v2

Figure 3. Dimensionless velocity pulsations of liquid near the impeller, $N = 6\ s^{-1}$.



(a) axial for $H^* = 0.380$ (b) radial for $H^* = 0.380$

(c) axial for $H^* = 0.297$ (d) radial for $H^* = 0.297$

(e) axial for $H^* = 0.200$ (f) radial for $H^* = 0.200$

Figure 4. Dimensionless profiles of axial and radial velocities and velocity pulsations under the impeller.

Just below the impeller ($H^* = 0.297$), the radial component of the velocity was close to zero, except for the impeller with a ring, for which there was a flow towards the wall with a maximum value of $U^*_{r\,\max} \approx 0.14$. The axial component increased almost linearly in the range of $R^*_h < R^* < 0.27$, and the maximum value was $U^*_{z\,\max} \approx 0.50$. Then the axial velocity decreased linearly and at the end of the vane was $0.1 \cdot U_{tip}$. Only for the impeller with a ring the maximum value of the axial component was lower and amounted to $U^*_{z\,\max} \approx 0.43$. The position of the maximum axial velocity is consistent with the literature information for the PBT impeller (Uhl and Gray, 1986).

The obtained velocity and velocity pulsation profiles under the impeller ($H^* = 0.297$) can be compared with the profiles described by Equations (4), (5), (6) and (7). This comparison is shown in Fig. 5.

The analysis of Fig. 5 shows that:

- the use of an airfoil profile has little effect on the course of the velocity and velocity pulsation profiles,
- the impeller hub has an effect on the velocity and velocity pulsation profile, which is not taken into account in Equations (4) and (5),

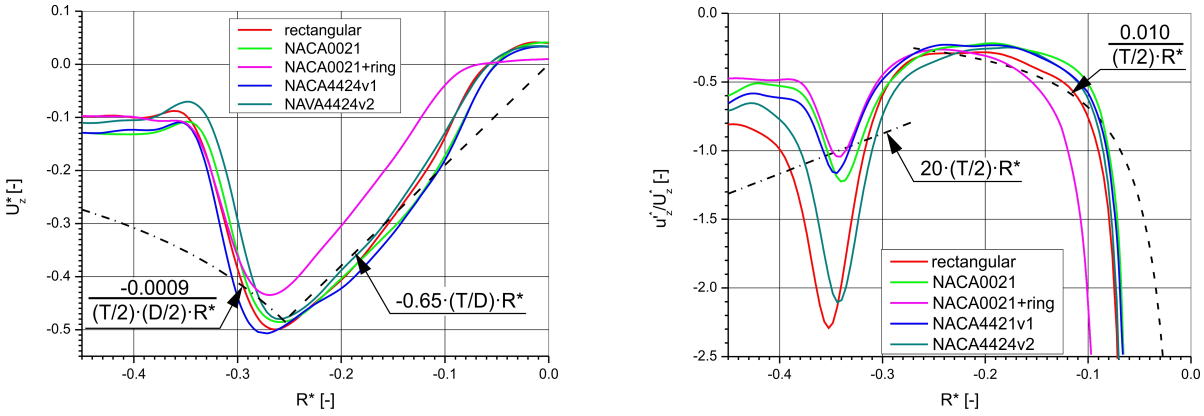


Figure 5. Comparison of dimensionless axial velocity and axial velocity pulsation profiles.

Table 1. Mean energy dissipation rates.

Blade cross-section	Eu	ε_m [m^2/s^3]			
		$N = 2$ s^{-1}	$N = 3$ s^{-1}	$N = 4$ s^{-1}	$N = 6$ s^{-1}
rectangular	1.580	0.006	0.021	0.050	0.170
0021	1.310	0.005	0.018	0.042	0.141
0021+ring	1.045	0.004	0.014	0.033	0.112
4424v1	1.410	0.006	0.019	0.045	0.152
4424v2	1.190	0.005	0.016	0.038	0.128

- for a radius smaller than r_c, Equations (4) and (6) describe the velocity and velocity pulsation profiles quite well, but the value of k deviates from the literature value of $k = \cot\alpha$, (for $\alpha = 45^\circ$ $k = 1$),
- for a radius greater than r_c, Equations (5) and (7) do not reflect the waveform of the velocity and velocity pulsation profiles.

Assuming the isotropy of the velocity pulsation allows to calculate from Equation (11) the distribution of the energy dissipation rate. The value of $C_2 = 5.2$ was used for the calculations (Stelmach, 2014). Values received were compared with the average value for the entire stirred vessel ε_m. Table 1 presents the calculated ε_m values obtained from the mixing power measurements (Gzowska, 2019).

Figure 6 shows the maps of energy dissipation rate distributions ε related to the average value for the stirred vessel ε_m. The red line indicates the value of $\varepsilon/\varepsilon_m = 1$.

The analysis of Fig. 6 shows that only under the impeller – in the stream of pumped liquid – the local values ε are higher than the average value. The highest values are observed at the lower end of the blade. The maximum value of $(\varepsilon/\varepsilon_m)_{\max} \approx 50$ occurred for an impeller with a rectangular blade cross-section. For the other impellers, this value was about 35. The obtained values of $(\varepsilon/\varepsilon_m)_{\max}$ are consistent with the literature information (Patterson et al., 2003).

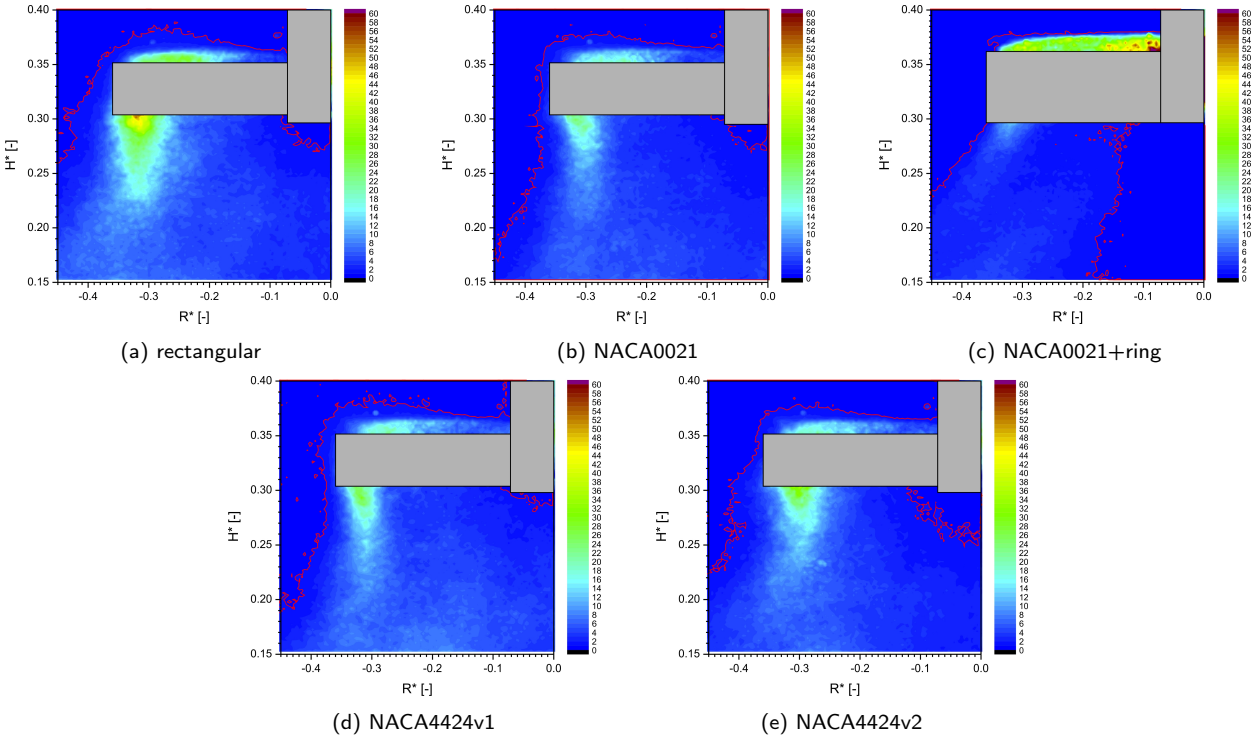
The data of the axial velocity profiles under the impeller were used to calculate the flow of liquid pumped by the impeller $\dot{V}_p$ and the pumping number Fl_p. Fig. 7 shows the results obtained. In the range of the Reynolds numbers under study, the constancy of the value of the pumping number Fl_p can be considered and the mean value for each type of impeller can be determined.

The obtained values of pumping numbers are smaller than the value calculated from the relation for the PBT impeller with rectangular cross-section of blade (Uhl and Gray, 1986)

$$Fl_p = 1.014 \cdot Re^0 \cdot \left(\frac{D}{T}\right)^{0.21} \cdot \left(\frac{H_m}{T}\right)^{-0.17} \qquad (12)$$

The value of Re^0 is of course 1, but the presence of this term in Equation (12) emphasizes the independence of the pumping number Fl_p from the Reynolds number Re. For the PBT impeller-stirred tank system tested in the work $Fl_p = 0.971$. The difference is probably due to the measurement methods, as Equation (12) was obtained indirectly by measuring the average time of the primary circulation using flow marks (flow followers). The possible impact of the measurement method on the Fl_p value is also evidenced by the value of $Fl_p = 0.793$ obtained in LDA measurements (Kresta and Wood, 1993).

Measurements of the axial force F_a were used to calculate the thrust numbers Th for the tested impellers. The results are presented in Fig. 8a. In the range of Reynolds numbers



(a) rectangular (b) NACA0021 (c) NACA0021+ring

(d) NACA4424v1 (e) NACA4424v2

Figure 6. Relative energy dissipation rate, $N = 6\ s^{-1}$.

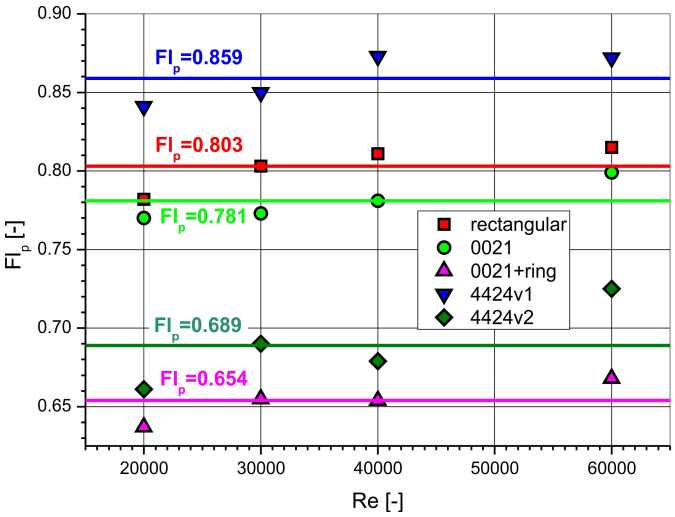


Figure 7. Dependence $Fl_p = f(Re)$.

under study, the constancy of the thrust number Th can be recognized and the average value for each type of impeller can be determined. Fig. 8b shows the relationship $Th = f(Fl_p)$.

Due to the small number of data, no correlation coefficients were determined for Equation (8). However, the graph shows a relationship $Th = 0.8 \cdot Fl_p^2$. A comparison of the curve with respect to the experimental points allows us to conclude that the value of $C_1 = 0.8$ given at the beginning allows for a good approximation of the experimental points.

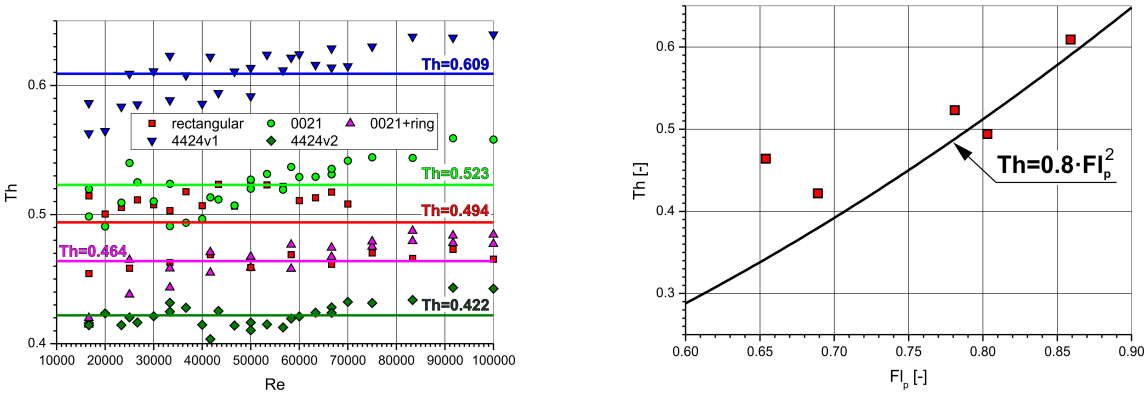
The values of the mixing power number Eu, the pumping number Fl_p and the thrust number Th are presented in Fig. 9a.

The efficiency values of the impellers calculated from the relationship Eu/Fl_p and Equation (1) are shown in Fig. 9b with the efficiency in relation to a standard impeller with rectangular cross-section of blades.

The impeller with a NACA4424 profile positioned with a less convex side in the direction of movement turned out to be the most effective. In this case, the impeller has a higher pumping capacity and a lower mixing power compared to a standard impeller. Also, the symmetrical NACA0021 profile gives more effective operation of the impeller compared to the rectangular profile. However, in this case, the efficiency is increased by significantly reducing the mixing power. In the case of large-diameter industrial impellers, the economic gain will be reduced by the higher cost of producing blades with an airfoil compared to blades with a rectangular cross-section.

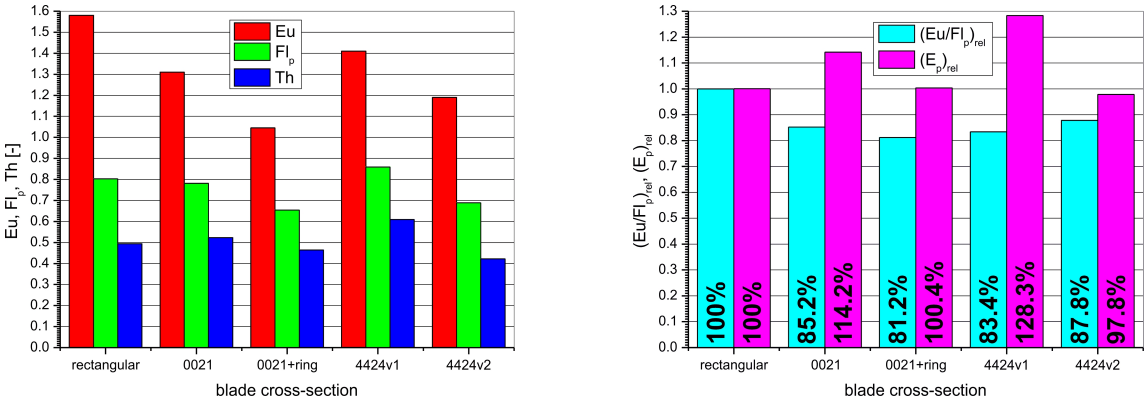
The PIV measuring system software allows you to calculate the Reynolds stress values. The results are presented in Fig. 10.

The stresses resulting from the fluctuation of fluid velocity do not exceed 200 Pa and are too small to destroy the cells of microorganisms. However, since the disintegration of microbial cells is observed in a mechanically stirred tank (Kuras, 2018), this should be attributed to the mechanical action of the impeller blades. According to the literature data, the Reynolds stress for the Rushton turbine (radial flow) determined in LDA measurements reaches a maximum value of 72 Pa (Galletti et al., 2004). The maximum value of τ_{RH} given in Galletti's paper reaches 46 Pa, which is comparable to the values from Figs. 10b and 10e.



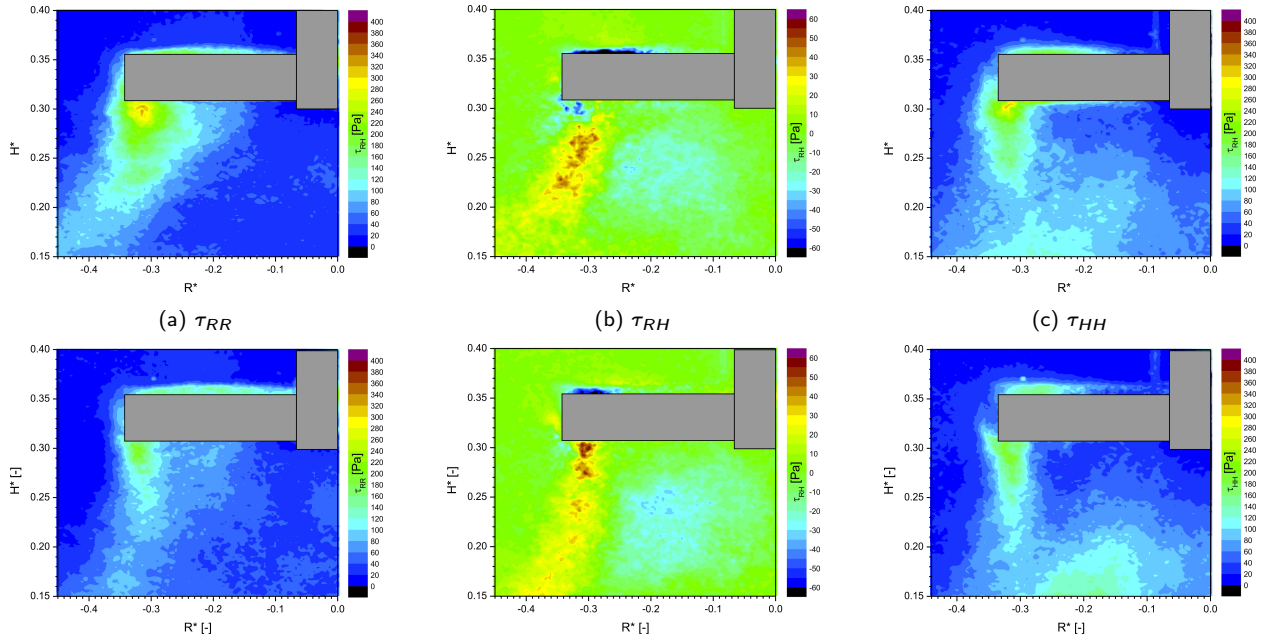
(a) (b)

Figure 8. Dependence $Th = f(Re)$ (a) and $Th = f(Fl_p)$ (b).



(a) (b)

Figure 9. Criterial numbers (a) and efficiency of the tested impellers (b).



(a) τ_{RR} (b) τ_{RH} (c) τ_{HH}

(d) τ_{RR} (e) τ_{RH} (f) τ_{HH}

Figure 10. Reynolds stress for a rectangular profile (a, b, c) and 4424v1 airfoil (d, e, f), $N = 6$ s^{-1}.

4. CONCLUSIONS

The use of airfoils can increase the efficiency of pitched blade turbine impellers with blades inclined at an angle of 45°. Among the shapes studied, the NACA4424 profile set with the less convex side in the direction of movement (like a load-bearing wing) turned out to be the best. Due to the increased cost of making blades with an airfoil, the economic viability of this design will be lower than the energy efficiency.

The use of a ring around the impeller blades changes the flow of liquid near the impeller, but does not increase its efficiency. There was also no significant reduction in impeller vibrations.

The highest energy dissipation rate and the highest stresses occur near the lower end of the blade.

The stresses associated with liquid pulsations in the liquid are too small to cause disruption of microbial cells.

The largest velocity pulsations were observed at the lower corner of the blade. Beyond this small area, the isotropy of velocity pulsations can be assumed.

In the area of the highest velocity pulsations, the energy dissipation rate was about 35 times higher than the average value for the entire mixer. On the other hand, outside the area under the agitator, the energy dissipation rates were lower than the average value.

ACKNOWLEDGEMENTS

Funding – the research was financed by the Department of Chemical and Molecular Engineering and Department of Sugar and Food Safety Management of the Lodz University of Technology.

SYMBOLS

c, C, C_1, C_2	coefficients, –
D	impeller diameter, m
B	baffle width, m
F_a	axial force, N
H_L	liquid height, m
H^*	dimensionless height (distance from bottom), $H^* = H/H_L$
H_m	distance between impeller and bottom of tank, m
K	coefficient, –
N	rotational frequency, s^{-1}
P	power, W
r	radius, m
r_c	radius for which the axial velocity reaches its maximum value, m
R^*	dimensionless radius, $R^* = r/(T/2)$
T	tank diameter, m
u'	velocity pulsation, m/s
U	velocity, m/s
U_{tip}	tangential velocity of tip blade, m/s
$\dot{V}_p$	pumping capacity, m^3/s

Greek symbols

α	attack angle (blade inclination angle), °
ρ	density, kg/m^3
τ	Reynolds stress, Pa

Subscripts

r	radial component
z	axial component
x, y, z	direction

Dimensionless numbers

Eu	power number, $Eu = P/(N^3 \cdot D^5 \cdot \rho)$
E_p	dimensionless efficiency, $E_p = \frac{\dot{V}_p \cdot \rho}{P \cdot T^4} = \frac{Fl_p^3}{Eu} \cdot \left(\frac{D}{T}\right)^4$
Fl_p	pumping (flow) number, $Fl_p = \dot{V}_p/(N \cdot D^3)$
Th	thrust number, $Th = F_a/(N^2 \cdot D^4 \cdot \rho)$

REFERENCES

Baldi S., Hann D., Yianneskis M., 2002. On the measurements of turbulence energy dissipation in stirred vessels with PIV techniques. *10th International Symposium on Applied of Laser Technique to Fluid Mechanics*, Lisboa, Portugal.

Delafosse A., Collignon M.-L., Crine M., Toye D., 2011. Estimation of the turbulent kinetic energy dissipation rate from 2D-PIV measurements in a vessel stirred by an axial Mixel TTP impeller. *Chem. Eng. Sci.*, 66, 1728–1737. DOI: 10.1016/j.ces.2011.01.011.

Fořt I., Seichter P., Peš L., 2013. Axial thrust of axial flow impellers. *Chem. Eng. Res. Des.*, 91, 789–794. DOI: 10.1016/j.cherd.2012.10.001.

Galletti C., Brunazzi E., Pintus S., Paglianti A., Yianneskis M., 2004. A study of Reynolds stresses, triple products and turbulence states in a radially stirred tank with 3-D laser anemometry. *Chem. Eng. Res. Des.*, 82, 1214–1228. DOI: 10.1205/cerd.82.9.1214.44151.

Głogowski M., Goszczak J., Stelmach J., Drożdż M., 2024. Research of an innovative mixer with reduced hydrodynamic resistance. *Adv. Sci. Technol. Res. J.*, 18, 142–155. DOI: 10.12913/22998624/193628.

Gzowska A., 2019. *Badanie mocy mieszania i hydrodynamiki nowego typu mieszadła do mieszania biozawiesin*. MSc Thesis, Lodz University of Technology.

Kresta S.M., Wood P.E., 1993. The mean flow field produced by a 45° pitched blade turbine: changes in the circulation pattern due to off bottom clearance. *Can. J. Chem. Eng.*, 71, 42–53. DOI: 10.1002/cjce.5450710107.

Kuras M., 2018. *Badania wpływu naprężeń tnących na dezintegrację komórek mikroorganizmów*. MSc Thesis, Lodz University of Technology.

Lebranchu A., Delaunay S., Marchala P., Blanchard F., Pacaud S., Fick M., Olmos E., 2017. Impact of shear stress and impeller design on the production of biogas in anaerobic digesters. *Bioresour. Technol.*, 245, 1139–1147. DOI: 10.1016/j.biortech.2017.07.113.

Linek V., Kordač M., Fujasová M., Moucha T., 2004. Gas-liquid mass transfer coefficient in stirred tanks interpreted through models of idealized eddy structure in the bubbly vicinity. *Chem. Eng. Process. Process Intensif.*, 43, 1511–1517. DOI: 10.1016/j.cep.2004.02.009.

Machado M.B., Nunhez J.R., Nobes D., Kresta S.M., 2012. Impeller characterization and selection: balancing efficient hydrodynamics with process mixing requirements. *AIChE J.*, 58, 2573–2588. DOI: 10.1002/aic.12758.

Mak A.T.-C., 1992. *Solid-liquid mixing in mechanically agitated vessels*. PhD Thesis, University College London.

Mashmoushy H., Zhang Z., Thomas C.R., 1998. Micromanipulation measurement of the mechanical properties of baker's yeast cells. *Biotechnol. Tech.*, 12, 925–929. DOI: 10.1023/A:1008825830928.

Nienow A.W., 1997. On impeller circulation and mixing effectiveness in the turbulent flow regime. *Chem. Eng. Sci.*, 52, 2557–2565. DOI: 10.1016/S0009-2509(97)00072-9.

Patterson G.K., Paul E.L., Kresta S.M., Etchells III A.W., 2003. Mixing and chemical reactions, In: Paul E.L., Atiemo-Oberg V.A., Kresta S.M. (Eds.), *Handbook of industrial mixing*, p.781. DOI: 10.1002/0471451452.ch13.

Paul E.L., Atiemo-Oberg V.A., Kresta S.M., 2003. *Handbook of industrial mixing: Science and practice*. John Wiley & Sons, Inc., New Jersey. DOI: 10.1002/0471451452.

Raffel M., Willert C.E., Wereley S.T., Kompenhans J., 2007. *Particle image velocimetry. A practical guide*. Springer, Berlin. DOI: 10.1007/978-3-540-72308-0.

Shiu C., Zhang Z., Thomas C.R., 1999. A novel technique for the study of bacterial cell mechanical properties. *Biotechnol. Tech.*, 13, 707–713. DOI: 10.1023/A:1008919915047.

Smith A.E., Zhang Z., Thomas C.R., 2000. Wall material properties of yeast cells: Part 1. Cell measurements and compression experiments. *Chem. Eng. Sci.*, 55, 2031–2041. DOI: 10.1016/S0009-2509(99)00500-X.

Stelmach J., 2000. *Badania pracy samozasysającego mieszadła tarczowego*. PhD Thesis, Lodz University of Technology.

Stelmach J., 2014. *Hydrodynamika układu dwufazowego ciecz-gaz w mieszalniku. Wykorzystanie metod fotooptycznych*. Monografie Politechniki Łódzkiej, Łódź.

Stelmach J., 2022. Wpływ profilu aerodynamicznego łopatek mieszadeł turbinowych o pochylonych łopatkach na moc mixingu zawiesin. *XII Ogólnopolska Konferencja Przepływów Wielofazowych*, Gdańsk, Poland, October 2022, 107–113.

Stelmach J., 2026. The influence of the shape of propeller impeller blades on hydrodynamics and efficiency. *Energies*, 19, 2146. DOI: 10.3390/en19092146.

Stelmach J., Kuncewicz C., 2017. Effect of propeller impeller blade profile on hydrodynamics and power consumption. *Przem. Chem.*, 96, 2348–2352. DOI: 10.15199/62.2017.11.25.

Stelmach J., Kuncewicz C., 2018. Naprężenia turbulentne w pobliżu mieszadła Rushtona. *Inż. Ap. Chem.*, 5, 150–151.

Stelmach J., Kurasiński T., Kuncewicz C., 2005. Analiza porównawcza wybranych metod obliczania szybkości dyssypacji energii. *Inż. Chem. Proc.*, 26, 201–215.

Stelmach J., Musoski R., 2017. Hydrodynamics in the blade region of a self-aspirating disk impeller. *J. Appl. Fluid Mech.*, 10, 1177–1188. DOI: 10.18869/acadpub.jafm.73.241.27124.

Stelmach J., Musoski R., Kuncewicz C., Glogowski M., 2019. Turbulent energy dissipation rate and turbulence scales in the blade region of a self-aspirating disk impeller. *J. Appl. Fluid Mech.*, 12, 715–728. DOI: 10.29252/jafm.12.03.28836.

Story A., Story G., Jaworski Z., 2021. Experimental and numerical investigation of axial and tangential forces in a stirred tank with yield-stress fluids. *Chem. Proc. Eng.*, 42, 173–190. DOI: 10.24425/cpe.2021.138923.

Stręk F., 1981. *Mieszanie i mieszalniki*. WNT, Warszawa.

Tanaka T., Eaton J.K., 2007. A correction method for measuring turbulence kinetic energy dissipation rate by PIV. *Exp. Fluids*, 42, 893–902. DOI: 10.1007/s00348-007-0298-y.

Uhl V.W., Gray J.B., 1986. *Mixing. Theory and Practice*. Vol. III, Academic Press, Inc., New York, 139–142.

Zlokarnik M., 2001. *Stirring: Theory and practice*. Wiley-VCH, Weinheim. DOI: 10.1002/9783527612703.